Space telescope for imaging Earth-like exoplanets in the mid-infrared

Engineering Case Study

A research study in cooperation with Netherlands Institute for Space Research in search for alien life in our Universe.

Abstract

This engineering report outlines the technical and engineering aspects of a proposed space telescope mission aimed at identifying and characterizing 25 temperate exoplanets orbiting sun-like stars. It covers details of the spacecraft's design, including guidance, navigation, control systems, thermal control, propulsion, electrical power subsystem, and attitude determination and control. The report also discusses the spacecraft's configuration, launch vehicle considerations, and cost estimation. The primary objective of this mission is to enhance our knowledge of habitable environments in our solar neighborhood and investigate the potential for extraterrestrial life, focusing on the engineering feasibility and technological advancements required for successful mission implementation.

Nomenclature

Acronyms

JWST	James Webb Space Telescope
BCS	Beam Combiner Spacecraft
TTC	Telemetry, Tracking and Command

Contents

1 Introduction

The quest to determine the presence and distribution of extraterrestrial life has been a driving force behind the exploration of celestial bodies within and beyond our solar system. The field of exoplanets, emerging in the mid-1990s, has provided a complementary approach to exploring other worlds. Over the past 25 years, it has become evident that exoplanets, especially terrestrial ones, are abundant and can be found around various types of nearby stars.

Advancements in technology now allow us to study terrestrial planets and their atmospheres using various observational methods. The ongoing exploration reveals a vast diversity of planets and planetary atmospheres, surpassing the variety observed within our own solar system. To further this exoplanet research, missions such as CHEOPS, JWST, and Ariel represent significant strides forward.

Collectively, these missions aim to conduct the first comprehensive survey of warm to hot exoplanet atmospheres, observing hundreds of objects. However, due to the inherent limitations of the primary observation methods, such as transit spectroscopy, the information gathered will remain quite restricted, especially for small terrestrial planets with temperatures low enough to potentially support liquid water on their surfaces. This limitation is particularly apparent when attempting to capture thermally emitted photons to explore regions near the planetary surface. Despite the challenges, studying these planets is crucial to gaining insights into the prevalence of habitable conditions in the broader universe.

The crucial exploration of temperate Earth-like exoplanets involves the pivotal task of directly detecting the infrared light emitted by their atmospheres. This approach is instrumental in unraveling the intricate chemical and physical diversity of these distant worlds and determining whether they truly harbor conditions conducive to supporting life.

This report focuses on the engineering side of the mission designed to find 25 temperate exoplanets. Utilizing existing technologies sourced from the James Webb Space Telescope and conceptual technologies from missions such as ESA's Darwin and LISA pathfinder. It will present the engineering concepts to be utilized for an interferometric infrared exoplanet detection mission.

2 Configuration

Contributed: Esther Koene
There are several configurations to be considered for a formation of spacecrafts used to apply nulling interferometry. Past studies have compared planar and non-planar flying and different aperture configurations. The following subsections will present various trade off tables for the configuration and the final choice for this project.

2.1 Aperture Configuration

The aperture configuration is the arrangement of the collector spacecrafts relative to each other and to the beam combiner spacecraft. Together with the relative phase differences between the received signals, it determines the angular receive characteristic of the nulling interferometer. Figure 1 shows schematics of the different aperture configurations and their nulling pattern.

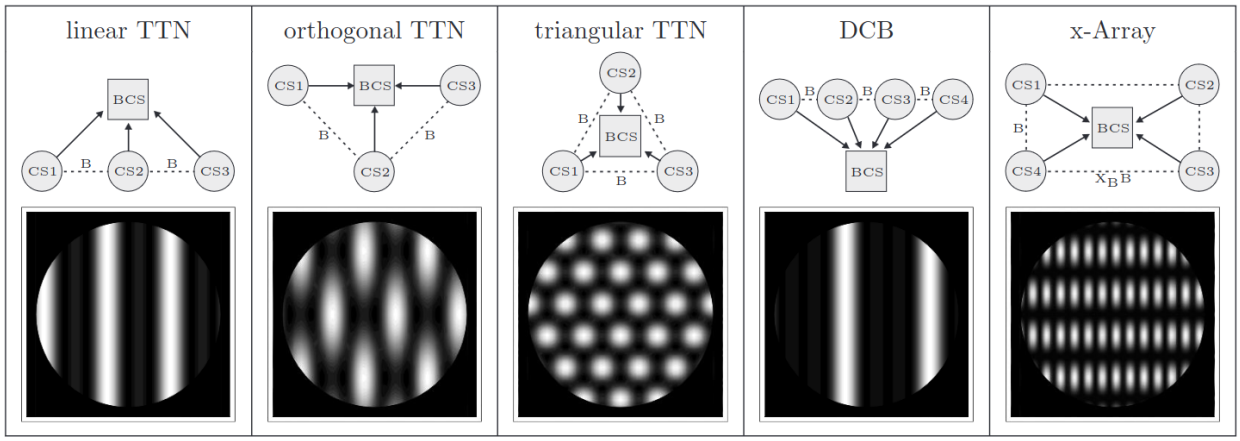

Figure 1: Aperture configurations for three and four telescope formations (TTN . . . three telescope nuller, DCB. . . dual-chopped Bracewell, CS. . . collector spacecraft, BCS. . . beam combiner space-craft, B . . . baseline, X_B . . . imaging to nulling baseline ratio. *Source:* [1]

To improve the performance of the nulling interferometer, two types of modulation are applied, namely array rotation and phase chopping. The latter is the technique of combining beams with different phases to produce two conjugated chopped states. These different states are then used to extract the planetary signal from the background [2]. Different modulation schemes to ensure efficient phase chopping are possible. The first column of table 1 shows the maximum of the modulation map for each three or four telescope nuller configuration. For the three telescope nuller options, the maximum of the modulation map is $\mathrm{M}_{Max} = 70\%$, taking an efficiency for 75% for beam recombination into account. The possible maximum for the four telescope nuller configuration is $\mathrm{N}_{Max} = 100\%$ [1].

Column two of table 1 shows the rotational modulation efficiency μ, which is a measure of how efficiently a planet is modulated by a certain aperture configuration. The values for the four aperture configurations, μ=34.9% for DCB and μ=28.8% for the x-array, are most favourable [1].

Column three of table 1 shows the Full-Width-Half-Maximum (FWHM) and the fraction F_{corr}. The FWHM quantifies the width of the correlation peak, which in turn quantifies the correlation of a planet signal with the signals from all possible planet locations within the field of view. If there is a single, sharp peak a less ambiguous and more reliable reconstruction of a planet's signal can be expected. In this category, the x-array configuration is with a FWHM of 38 mas the best option. F_{corr} quantifies the fraction of the field of view

where the correlation is higher than 50%. This allows us to evaluate the influence of sidelobes of the correlation peaks, which are weak compared to the main peak in the ideal case. Once again, the x-array shows the most promising value [1].

	Phase chopping	Array rotation	Reconstruction	
			FWHM	F_{corr}
Linear TTN	$M_{Max} = 70\%$	$\eta = 24.3\%$	317 mas	5.8%
Orthogonal TTN	$M_{Max} = 70\%$	$\eta = 19.5\%$	86 mas	1.0%
Triangular TTN	$M_{Max} = 70\%$	$\eta = 17.9\%$	72 mas	4.3%
DCB	$M_{Max} = 100\%$	$\eta = 34.9\%$	350 mas	5.6%
x-array	$M_{Max} = 100\%$	$\eta = 28.8\%$	38 mas	0.8%

Table 1: Trade off table with modulation and reconstruction characteristics for three and four aperture configurations

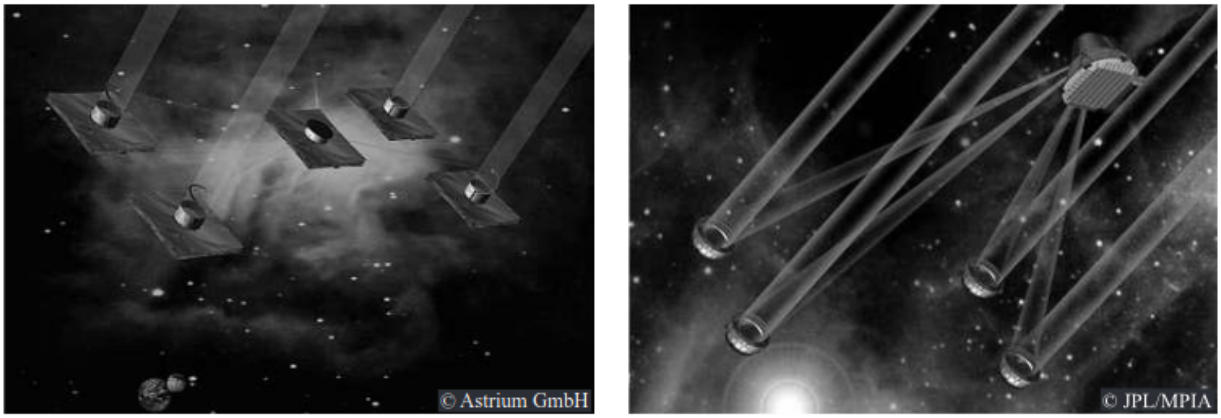

Figure 2: Artistic views of a planar (left) and a non-planar (right) spacecraft formation for a nulling interferometry mission.

2.2 Planar versus non-planar

Due to the unwanted effects of stray light, the three or four collector spacecrafts have to be arranged in one plane. The beam combiner spacecraft may be arranged in the same plane or above the collector spacecrafts, forming the non-planar configuration (see figure 2). In case of the latter, large mirrors on the collector spacecrafts reflect incoming light, focusing it onto receive optics of the beam combiner spacecraft which is situated about 1000 meters above the collector spacecraft [1]. Table 2 shows a trade off between the planar and the non-planar configuration. The first column shows the ecliptic latitudes the different formations can access. The non-planar can access a region of $\pm$ 72 °, which corresponds to 36% more targets from the DARWIN target catalogue [3].

Deep nulling has various requirements that can be met more easily through a symmetric configuration, requiring far less intricate engineering compared to an asymmetric setup. As per the second column, the beam routing scheme for the planar configuration is inherently symmetric, while the non-planar configuration is not. Non-planar configurations would need huge technological developments, while there are well established concepts for the planar formations (included in table 2, column three) [3].

The fourth column of table 2 covers another challenge for formation flying: the control of stray light. Specular reflection and thermal emission of the collector spacecraft receive optics and scattering and diffraction at all sunshields are all major sources of stray light. The advantage of non-planar formations is that the beam combiner spacecraft can only see the cold side of the sunshields and that it is far away (typically 1000 meters). However, with properly designed baffels and multi-layer sunshields, stray light can be rejected to acceptable levels for planar formations as well [3].

	Ecliptic latitudes	**Beam routing**	**Instrumentation**	**Stray light control**
Planar	± 45 °	Symmetric	Established concepts	Needs proper baffles/sunshields
Non-planar	± 72 °	Asymmetric	Needs development	Beam combiner is far away

Table 2: Trade off table for the planar versus non-planar configuration

2.3 Configuration of choice

After careful consideration of the trade offs mentioned in table 1 and table 2, the non-planar x-array (four collector spacecraft) configuration was chosen for this project. The x-array configuration clearly shows the best performance with regards to modulation and reconstruction characteristics. While the symmetrical planar configuration requires less intricate engineering and less technical development, the advantages in performance of the non-planar formation justify the extra time and resources needed to develop this possibility. However, the planar x-array will be available as a backup in case of unforeseen technical obstacles.

3 System Breakdown

3.1 Guidance, Navigation and Control

Contributed: Pieter van Zoelen
One of the stakeholder requirements is that the satellites orbit near the second Sun-Earth Lagrange point, L2 ([STA-04]). This is a point where the combined gravity of the sun and earth allow objects to have the same angular velocity as the Earth despite being further from the Sun. Doing so allows a single heatshield to reflect heat from the Sun, Earth and Moon. This point, however, does not allow for dynamically stable orbits. Lissajous orbits however are possible, which *appear* to be periodic orbital trajectories. In practice, they are not quite stable due to external disturbances. Nevertheless, these trajectories are cheaper to maintain in terms of Δv than other trajectories around L2.

Inspired by JWST, we want to have a trajectory in which the sun is never eclipsed. This simplifies the electrical and thermal subsystems, because we don't need to store energy to operate during eclipses and no thermal cycling occurs after launch. While most Lissajous orbits still pass through the Earth's shadow periodically, a subclass of Lissajous orbits called halo orbits can be done in such a way that they have no possibility of passing through the eclipse.

The size of the orbit determines how large the sunshield needs to be to avoid stray light from both the Earth and Sun, and how much stationkeeping Δv is needed. Larger orbits decay slower, but also require a larger sunshield. Because we lack the resources to do detailed trajectory simulations, we have chosen to use the same orbit as JWST, which has a stationkeeping budget of 26.0 m/s designed to last 10.5 years [4]. Controlling relative distances between satellites is discussed in section 3.5.2.

The launch vehicle can deliver the satellites directly to an L2 transfer orbit, and L2 insertion itself is free. To account for launch vehicle performance variations, JWST had 57.9 m/s of Δv for mid-course corrections [4]. Since we use the same orbit, we can expect to need the same.

Based on these values, we will need 70.3 m/s of Δv if the mission needs to last 5 years, and only 13.6 m/s extra to be able to extend that to 10.5 years. This does not include the budget for being able to delay the course corrections, doing so would increase the budget by 12.6 m/s. Including everything the total budget is 96.5 m/s.

To track the satellites we can use the DSN S-band tracking service. Because of the complex and unstable trajectory and relatively low velocity relative to Earth we need to track for around 19 days to accurately determine the current trajectory [5]. This means that stationkeeping maneuvers need to be spaced apart at least that much to be able to determine the effect of the maneuvers. The distance between satellites can be determined with Formation Flying Radio Frequency using multiple antennas for 50 cm distance accuracy at distances between 16 and 10000 meter, and laser interferometry on the micrometer to nanometer scale [6]. Bearing accuracy is provided with FFRF at 1°.

3.2 Attitude Determination and Control System

Contributed: Jasper Welgemoed
In order to obtain and maintain a pointing accuracy that enables us to take stable images of the objects we want to observe, we need an attitude determination & control system. This system consists of a functional flow between attitude determination sensors, attitude actuation devices, algorithms to determine attitudes and accountance for disturbance torques. This process can be viewed in the figure below. First the determination will be discussed, then the pointing stability, the disturbances that can influence this stability and lastly the attitude control system.

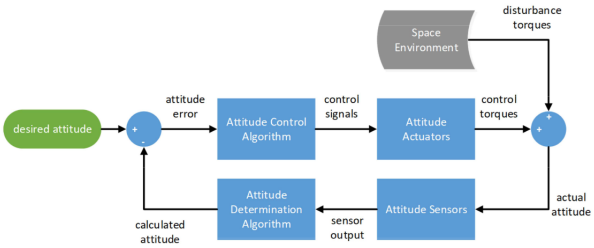

Figure 3: Attitude Determination and Control Flow Diagram

3.2.1 Attitude Determination

Contributed: Jasper Welgemoed

The first step is to determine the attitude. For this, we need to know how well our attitude needs to be determined. A body-fixed reference is chosen as a reference frame for each spacecraft. Now with respect to this we can determine the attitude with sensors which will be traded-off below. It is important to make the distinction between determination accuracy and control accuracy as these accuracy errors add up to each other. First the attitude determination will be discussed, but for this, we need to know how accurately we need to determine our attitude.

Pointing Accuracy For the pointing accuracy we are limited by the minimum separation distance of the exo-planet to the star at our maximum observation distance. For our minimum angular resolution at a minimum habitable zone separation distance of 1AU at a maximum observation distance of 18.26pc we get $\theta = \frac{d}{D} = 0.05''$. Luckily this is only the resolution and not the accuracy we need to attain as our field of view is larger than that namely comparable to the Darwin proposal of 1 arcsec^2. This means that in order to maintain this resolution within the field of view, we can move around 0.95" in x and y direction before our target gets out of the field of view. In order to maintain a resolution of $0.05''$ within our field of view, we can not afford attitude determination errors of larger than 0.95 arcsec in x and y direction. A table with possible determination sensors are given below. Typical accuracies as well as some general prices for these sensors are provided by NASA [7].

Table 3: Trade-off table for attitude determination options

Type of Sensor	Accuracy	Cost (euro)	Required input availability
Magnetometer	1 degree	15000	Not available at L2
Earth Horizon Sensor	0.1 degree	10000	Too far away to measure horizon
Sun Sensor	0.01 degree	3300	Sun is always at the back of the spacecraft
Star Tracker	0.001 degree	50000+	Available
Fine Guidance Sensor	0.1 as to 25mas	?	Available

At the distance of the L2 orbit, the magnetometer and earth horizon sensor would not be of good use since the magnetic field of the earth is too faint maintain to enough accuracy and the earth's horizon is too far away to maintain enough accuracy. The sun sensor would also not be of good use since it's always fixed behind the spacecraft in the L2 orbit. Star trackers are suitable for an initial estimation of our attitude, but in order to determine our attitude within our boundaries it leaves us only with the Fine Guidance Sensor. I want to add here that together with the communications engineer, we found that the star trackers by them self are already of sufficient accuracy to determine the attitude of the high-gain and medium-gain communication antennas towards the earth. [8].

The Fine Guidance Sensor makes use of astronomic accuracy of guidance stars in the Guidance Star Catalog. The sensor uses 5 software functions to get the attitude determination accuracy up to 25 milli-arcseconds depending on how accurate the guidance star location is known. The first function is the calibration where a full-frame picture is taken from the sky and a guidance star is selected. Then the sensor goes to the identification state where the selected guidance star is centered in the FGS detector and the science target (star) is in the field of view of the instrument detect. Then it moves to the acquisition state where the guide star is centered in a sub array of $8.8'' \times 8.8''$. This information is sent to the attitude control system and is simultaneously analysed. Then a sub-array of $2.2'' \times 2.2''$ is centered in the guide star to update the ACS knowledge.

The ACS reacts to this offset and repeats this step every 64ms in the tracking state to bring its accuracy down from 0.1" to 0.06". Once this accuracy is achieved, the final state is achieved which is the fine guide. A sub-array of $0.5'' \times 0.5''$ is placed in the center of the star every 64ms while controlling the attitude in a closed loop[9]. In this final state, the pointing accuracy can be increased to values up to 25 mas depending on the initial accuracy of the star's location documented in the Guidance Star Catalog [9]. This is well within our accuracy limit.
While the price is unknown for the fine guidance sensor, we are required to use it and it should have a big priority in our budget. Since the back of the 4 telescopes and the beam combiner will be pointed towards the sun at all times, we will provide every telescope with 2 star trackers and 2 fine guidance sensors for each telescope and the beam combiner. Each at 90 degrees from each other in the telescope's field of view. For redundance we could choose to use 3 of each on each telescope and beam combiner.

Pointing Stability For the pointing stability we are limited by the width of the fringes that occur with the interferometry. This can be influenced by jitter or vibrations of the actuators or any mechanical, thermal electrical disturbance. The width of these fringes are given by $\lambda/(2b)$, where λ is the wavelength and b is the length of the baseline. For the worst-case scenario, our wavelength is 25microns and our baseline is around 100 meters. We get a fringe distance of $d = \dfrac{25 \cdot 10^{-6}}{100} = 25 \cdot 10^{-8} m$. This means that any movement greater than this number, results in a shift of fringes. Which means that the star will end up in the constructive part of the interferometry and the planet in the destructive zone. These disturbances can only be limited but never neglected. Over a maximum distance of 18.26pc there is no attitude controller accurate enough to stay within this fringe width. So we need something else. One commonly used solution is a Fast Steering Mirror in combination with a Fine Guidance Sensor. Instead of trying to stabilize the spacecraft to jitters smaller than the fringe distance, we try to stabilize the beam after it has hit the mirror. Behind the mirror we can still alter the optical path difference of the beams (the phase) as well as the stability of these optical path differences which can alter the fringes. This FSM will be implemented in a closed loop in the attitude control system together with the Fine Guidance Sensor. The FSM will be constantly moving in X- and Y-axis trying to stabilize the beam in order to keep the fringes stable as well as the overall image. The JWST uses a FSM that has an optical performance of between 60nm-80nm [10]. Which is well within our maximum range of the fringe width.

3.2.2 Disturbance Torques

Contributed: Jasper Welgemoed
In L2 orbit, we undergo various disturbance torques which affect the attitude of our spacecraft. Most of these are small and periodic, yet need to be accounted for long missions like ours. If we calculate the resulting torques of these perturbations and take them into account together with our maximum exposure time, we can calculate how much effect they have on our pointing stability during one exposure. Note that these are very rough estimations and one dimensional in the worst-case scenarios.

Magnetic Disturbance Torque This effect is calculated with the residual dipole moment of the spacecraft and a magnetic field that influences the magnetic disturbance the most, which would in our case be the earths magnetic field. For the worst case when the dipole and the magnetic field are perpendicular, the disturbance torque can be calculated as $\tau_m = D_{res} \cdot B$ with $B = 2M/R^3$, $M = 8 * 10^{15}$ Tm^3 being the magnetic field of the earth and $R = 1.5 \cdot 10^9$ m the distance from earth to L2 orbit altitude. Assuming the residual dipole moment between 0.1 Am^2 and 20 Am^2 we find an average disturbance torque of $\tau_m \approx 10^{-12}$ Nm.

Gravitational Disturbance Torque This effect can be calculated through $\tau_g = \frac{\mu}{2R^3} \cdot |I_{max} - I_n| \cdot \sin(2\theta)$ with $\mu = 3.968 * 10^{14}$ m^{3}s^{-2} and R as the distance from the L2 orbit to the gravitational body. I_{max} is the maximum moment of inertia and I_n the smallest moment of inertia perpendicular to I_{max}, θ is the angle between the local vertical and the I_{max} axis. Assuming $I_{max} - I_n$ to be in the order of 100 kg m^2 (order of a larger more complex satellite)[7]. We get a torque roughly of the order 10^{-11} Nm. This is only for the earth and the influence of the moon and sun can be calculated in a similar way.

Solar Disturbance Torque This effect is expected to have the largest impact on our spacecraft in L2 orbit. It is calculated through $\tau_s = \frac{q_{sun}}{c} \cdot A_s \cdot (2 - \alpha) \cdot \cos(\theta_i) \cdot (c_{ps} - c_m)$. Here $q_{sun} = \frac{L}{4\pi r^2} = \frac{3.838 * 10^{26} W}{4\pi \cdot (1.5 \cdot 10^9 m)^2} \approx 1354$ Wm^{-2} is the solar flux at the L2 orbit and c is the speed of light. Where A_s is the surface area of the lighted side of the space craft, which in our case would be only the back side, which has a maximum surface area of the diameter of the sun shields which are larger than the mirror so > 2.5 m and α is the absorption coefficient. $\theta_i \approx 0$ is the incidence angle of the incoming light with the surface as we are always with our back towards the sun. We want to minimize the distance between the center of pressure c_{ps} and the center of mass c_m. Assuming $c_{ps} - c_m$ in the order of 10^0 we get an estimate of the solar pressure perturbation torque in the order of 10^{-4} Nm.

3.2.3 Angular Displacement

These torques result in a displacement of the spacecraft which can effect our pointing accuracy if it's not accounted for. This displacement can be calculated with the maximum time it needs to be in fine guidance mode. Which is worst-case with our longest exposure time of 1 day 1 hour and 26 seconds without overhead. From $\alpha = \frac{\tau}{I}$ we can get our angular acceleration assuming the torque is constant. Assuming an initial angular velocity of $\omega_0 = 0$ we can calculate the angular displacement with $\theta = \frac{1}{2}\alpha t^2$ again for constant torque. Assuming our moment of inertia to be of the order 100 kg m^2 [7]. We get magnetic, gravitational and solar angular accelerations of $\alpha_m = \frac{10^{-12}}{100} = 10^{-14}\frac{rad}{s^2}$, $\alpha_g = \frac{10^{-11}}{100} = 10^{-13}\frac{rad}{s^2}$, $\alpha_s = \frac{10^{-4}}{100} = 10^{-6}\frac{rad}{s^2}$ respectively. Over a time of 91560 seconds this results in a magnetic torque displacement of $\theta_m = 0.000041916° \approx 0.15090''$ which is within our accuracy limit, so it does not necessarily need to be accounted for. For $\theta_g = 0.00041916° \approx 1.50898''$ which is above our limit so needs to be accounted for with attitude controllers of which a suitable one will be discussed later in this chapter. For $\theta_s = 419161.68° >> 0.95''$ we see that the solar disturbance results in the biggest effect. It makes the spacecraft tumble around its axis 0.8 times per minute. This means we need constant coarse attitude control for maintaining the attitude.

3.2.4 Attitude Control

Now that we can determine our attitude to an accuracy between 0.1 arcsec and 25mas and our maximum pointing inaccuracy can be 0.95 arcsec. We need to pick actuators that can control the attitude of the spacecraft between 0.85 arcsec and 0.925 arcsec in x and y direction. We need to make a distinction between the initial "coarser" attitude changes and the fine changes needed for the required accuracy. For this, we can use multiple controllers simultaneously. A trade-off table is provided below. The typical accuracies and prices for these actuators are provided by NASA standards in documentation [7]

Table 4: Trade-off table for attitude determination options

Type of Actuator	Accuracy	Cost (euro)	Required input availability
Magnetotorquer	1 degrees	15000	Not available at L2
Reaction Wheels	fine changes	20000	Available
Thrusters	coarse changes	1000000	Available

In theory it would suffice to only use reaction wheels, but as perturbations accumulate over time, it is important to dump momentum from time to time. Otherwise the reaction wheels can become saturated. We could choose to dump momentum after each exposure. Since magnetotorquers are not available at L2 orbit, we are required to use thrusters. Even though they are the most expensive, they are required. They are less accurate than reaction wheels, but can be used for the more coarser attitude changes and quick re-orientations. The type of thrusters used is explained in the Propulsion section. We will use the same thrusters that are used for the coarser orbit control changes. Since $\tau = F_t \times r$ where r is the distance from the center of thrust and the center of mass, F_t is the thrust and τ is the torque required. We can assume r to be of order 10^0 we find $F_t \approx 10^{-4} N$ and therefore that the micronewton thrusters used for orbit control are sufficient to counteract the solar pressure perturbations. For the smaller torques and fine steering, we need more accurate controllers like reaction wheels. We can control all these controllers with PID control loops and attitude control algorithms.

$$T_c(t) = K_{\mathrm{p}} e(t) + K_{\mathrm{i}} \int_0^t e(\tau)\, d\tau + K_{\mathrm{d}} \dot{e}(t),$$

The control torque T_c depends on the proportional, integral and deviation parameters K_p, K_i, K_d and e is the attitude deviation signal that is the error between the FSG determined attitude and the required attitude. With control theory, the parameters can be tweaked to gain the highest accuracy and least bias, but this needs extensive iterations that goes beyond the scope of this project. With the input of the fine guidance sensor, we can put the controllers in a closed loop with the payload to obtain the accuracy we need. For full attitude control on all axis, we need 12 thrusters divided into 3 modules each with 4 thrusters. This will cost millions, but it is necessary as no other form of actuation like magnetotorquers are available, so we need to prioritize the thrusters in our budget. We can use the same thrusters as the ones controlling the orbit.

In order to minimize the effects of the perturbation torques, we can also choose to implement gyroscopic stiffness by introducing an initial angular momentum big enough to keep the spacecraft from accumulating too much perturbations from the solar pressure. This can be done by adding momentum wheels. One downside of this added stiffness, is that this would severely hinder the maneuverability of the spacecraft. Which is a problem for using our different pointing modes.

3.3 Telecommunications

Contributed: Berke Salar

The determination for the telecommunications system requires by first referencing existing telecommunication systems present in satellites in the L2 point. The JWST broadcasts primarily in the Ka-band (26.5 to 40 GHz) for the transmission of scientific data, which is suitable for higher bandwidth telecommunication. For telemetry and telecommunications the JWST transmits in the S-band (2 to 4 GHz), which is less suitable for high bandwidth telecommunication [11]. These carrier frequency bands, which fall under radio-waves, are of particular interest due to the transmittance of the Earth's atmosphere to radio-waves. Bands at higher frequencies and radio-waves with long wavelengths are largely blocked by the Earth's atmosphere, making telecommunication in these band impractical [12].

For primary data-telecommunication the Ka-band is selected. The system is sized for optimal directivity at a frequency of 27.5 GHz. The primary communications antenna onboard the JWST is a high gain, 60cm Ka band antenna. At Earth NASA's Deep Space Network (DSN) 70m telescopes can be utilized for communications. These are located in California, Spain and Australia and allow for a continuous line of sight towards the array.

Using the equations for the link-budget, referring the ratio between the receiving (P_{RX}) and transmitting (P_{TX}) powers in Equation 1. With λ_c the carrier wavelength and d the distance between the array and a receiver station. The signal power loss or the ratio between transmit and receive power is estimated to be 123 [dB] for this system.

$$\frac{P_{RX}}{P_{TX}} = \frac{G_{Ant-TX}G_{Ant-RX}}{L_{FS}L_{Atm}} \qquad G_{Ant} = \frac{4\pi A_{eff}}{\lambda_c^2} \qquad L_{FS} = \left(\frac{4d\pi}{\lambda_c}\right)^2 \tag{1}$$

Next is determining a minimum receive power. This largely depends on the selected (binary) coding scheme, a preferred maximum Bit Error Rate (BER) and the specifics of the receive circuit. Let the system be sized for a simple modulation scheme, such as Amplitude Shift Keying (ASK). Using a BER of 10^{-9} which is commonly preferred for satellite communication and assuming an ambient temperature of the receive antenna as 290 [K] along with an equivalent receiver system noise temperature of 100 [K] one can find the system noise power spectral density (N_0) with Equation 2. This equates to be $5.38 \cdot 10^{-21}$ [W Hz^{-1}].

$$N_0 = kT_{tot} \text{ [W Hz}^{-1}\text{]} \tag{2}$$

Then for ASK the Bit Error Rate is defined to be: BER $= P\left[Z \geq \left(\sqrt{\frac{P_{signal}}{2N_0 B_{eq}}}\right)\right]$, where Z is a standard normally distributed random variable ($Z \sim N(0,1)$) [13]. For BER $= 10^{-9}$ and a bandwidth (B_{eq}) equivalent to that of the JWST, being $B_{eq} = 3.5$ [Mhz], a receive signal power of at least $1.08 \cdot 10^{-11}$ [W] is required. Referencing this to the input, using Equation 1, the transmission signal power should be at-least 22.1 [W]. However a 3 [dB] overhead should be applied to account for unforeseen attenuations and inaccurate pointing of the satellite antenna, thus the satellite antenna should be specified to 44.1 [W]. The array should still be reachable in case the 70m antenna is unavailable, as such the 34m antenna could be utilized. This however requires a transmission power of 116 [W] with an overhead.

The JWST further employs a medium gain S-band antenna's for telemetry, these are specified as 0.2m with a down-link bandwidth of 40 [KHz]. The minimum transmission power should be 6.2 [W] for 70m receive antenna and 26.4 [W] for the 34m antenna.

With these specification a configuration must be selected. Referring to the trade-off table in Table 5 it can be seen how the configurations are rated. Configuration 3, where every satellite in the array contains a high- and low-gain antenna, is the most costly but at the same time is most reliable. Configuration 3's main advantage is that when one of the satellite antenna is out of commission the others can transmit the scientific data or telemetry instead. However due to the high costs this approach is not favoured. Configuration 2 only accounts for redundancy in the medium gain antenna. Configuration 1 has the lowest reliability of the 3 configurations, employing no redundancy. This reliability is comparative however, antenna onboard satellites are quite reliable. Configuration 2 is seen as most preferable since its a good trade-off between redundancy, direct communication to the mirrors and the power-budget. Aside from the S- and Ka-band antenna's the array should also be provided with a 5 Watt S-band low-gain omnidirectional antenna to allow for inter-satellite communication.

Table 5: Trade-off for different array satellite configurations, stipulating the antenna allocation to the beam combiner and telescope satellites.

	Ka-band antenna	**S-band antenna**	**Power cost [W]**	**Reliability**
Config 1	1 for the Beam-combiner	1 for the Beam-combiner	Beam-combiner: 148 Telescope: 5	Comparatively low
Config 2	1 for the Beam-combiner	1 for the Beam-combiner and 1 per telescope	Beam-combiner: 148 Telescope: 31.4	Good
Config 3	1 for the Beam-combiner and 1 per telescope	1 for the Beam-combiner and 1 per telescope	Beam-combiner: 148 Telescope: 148	Great

3.4 Command and Data Handling

Contributed: Esther Koene

To collect, process, route, store and down-link on-board generated data and to route and store up-linked data the mission will need an on-board data handling system (OBDHS). The on-board data handling system will be situated in the Beam Combiner Spacecraft (BCS).

The first choice that has to be made for the design of the OBDHs is between three types of architectures: centralized, bused or networked. Each architecture has several advantages and disadvantages, some of which depend on whether the system would be considered small or large. The advantages and disadvantages of the different architectures, considering a small system, are summarized in table 6.

	Data rates	**Monitoring**	**Complexity**	**Scalability**	**Fault tolerance**
Centralized	High	Difficult	Simple	Low	Medium
Bused	Limited	Easy	Simple	High	Medium
Networked	High	Difficult	Complex	High	Good (distributed)

Table 6: Trade-off for different system architectures [14]

There are a few points to consider when looking at the trade-off table. Firstly, the complexities of the bused and networked architecture depend on the bus and network interface respectively. If these interfaces are well designed, these architectures work well for small systems as well as large systems. Secondly, we have to consider how faulty devices are handled. In a bused architecture, a faulty device jamming the bus communication may be difficult to isolate. In a network, a faulty device could block other communication. An advantage of the network architecture, however, is that the fault tolerance is distributed.

An important aspect of the bused option is the standardized interface to all units and subsystems, which makes it easy to integrate and test.

After considering all of the pros and cons, the bused architecture was chosen for this project.

3.4.1 Architectures

Data architecture

In order to design the data architecture for the spacecraft, a few calculations have been made using the observation dimensions mentioned in the proposal for the DARWIN mission [15]. Table 7 shows how much data is produced using a bit depth of 16. These numbers are used in table 8a and 8b, which show the total data produced in example observations of 60 minutes with a sample rate of 12. These numbers were once again used to find how much data would need to be downlinked to the Deep Space Network, averaging every 10 frames and using a compression factor of 0.7 (see table 9a and 9b).

Following requirement [STA-06], the datalink budget for this project is 235 Gigabits that get downlinked to the Deep Space Network per day, which is the datalink budget of the James Webb Space Telescope [16]. Using this budget, the number of observations per day that would be possible with the example datarates are added to tables 8a, 8b, 9a and 9b. With a duration of 60 minutes, the number of observations that could be downlinked would of course be limited by, not even taking overhead into account. However, these numbers show that with these estimations, data of mid-IR detection would not have to be averaged or compressed, nor stored on board long term. The bit depth, sample rate or the dimensions could be increased and there would still be no need for on board storage. Further research will have to be conducted to find the optimal values for these variables. For the imaging function, the maximum number of observations per day is four if the frames are not averaged and if the data is not compressed, meaning one or both of those processes is necessary.

Observation Data Produced				
Data Product	Dimensions	Total value	Bits	Total bits (Mb)
Mid-IR detector	500 x 8	4000	16	0.064
Imaging	300 x 300	90000	16	1.44

Table 7: Projected observation data produced.

Example Observation mid-IR detector	
Duration	60 min
Data / sample	0.064 Mb
Sample rate	12
Total data	2764.8 Mb
Observations per day	85

(a) Mid-IR detection

Example Observation imaging	
Duration	60 min
Data / sample	1.44 Mb
Sample rate	12
Total data	62208 Mb
Observations per day	4

(b) Imaging function

Table 8: Total data produced in an example observation.

Downlinking example observation mid-IR detector	
Data stored	2764.8 Mb
Averaging	Every 10 frames
Compression factor	0.7
Data to downlink	193.5 Mb
Observations per day	1214

(a) Mid-IR detector

Downlinking example observation imaging	
Data stored	62208 Mb
Averaging	Every 10 frames
Compression factor	0.7
Data to downlink	4354.6 Mb
Observations per day	54

(b) Imaging function

Table 9: Data to downlink for an example observation.

Hardware architecture

Figure 4 shows a first design of the hardware architecture. The choice to keep platform data and payload data separate stemmed from the differing data rates and levels of criticality of the two. Platform data is transferred via the Remote Terminal Units (RTU's) to the data bus, which in turn transfers it to the Central Command and Telemetry Unit (CCTU). The CCTU connects to the transceiver, which receives from and transmits to ground control. The CCTU also connects to the on-board computer, which is responsible for security, on-board time management and distribution, spacecraft health monitoring, fault detection isolation and recovery, execution of command schedules and execution of control algorithms. For the BCS data bus, the MIL-STD-1553 was chosen as it is a sector standard widely used in spacecraft on-board data handling system, including on the JWST. Payload data is processed and transferred to the transceiver via the SpaceWire router. SpaceWire was chosen mainly for the data rates of its radiation tolerant devices: 200 Mbit/s data

signalling rate with a data-rate of 160 MBit/s per link or 152 Mbit/s bi-directional per link [17]. These data rates should prove sufficient for transferring of payload data.

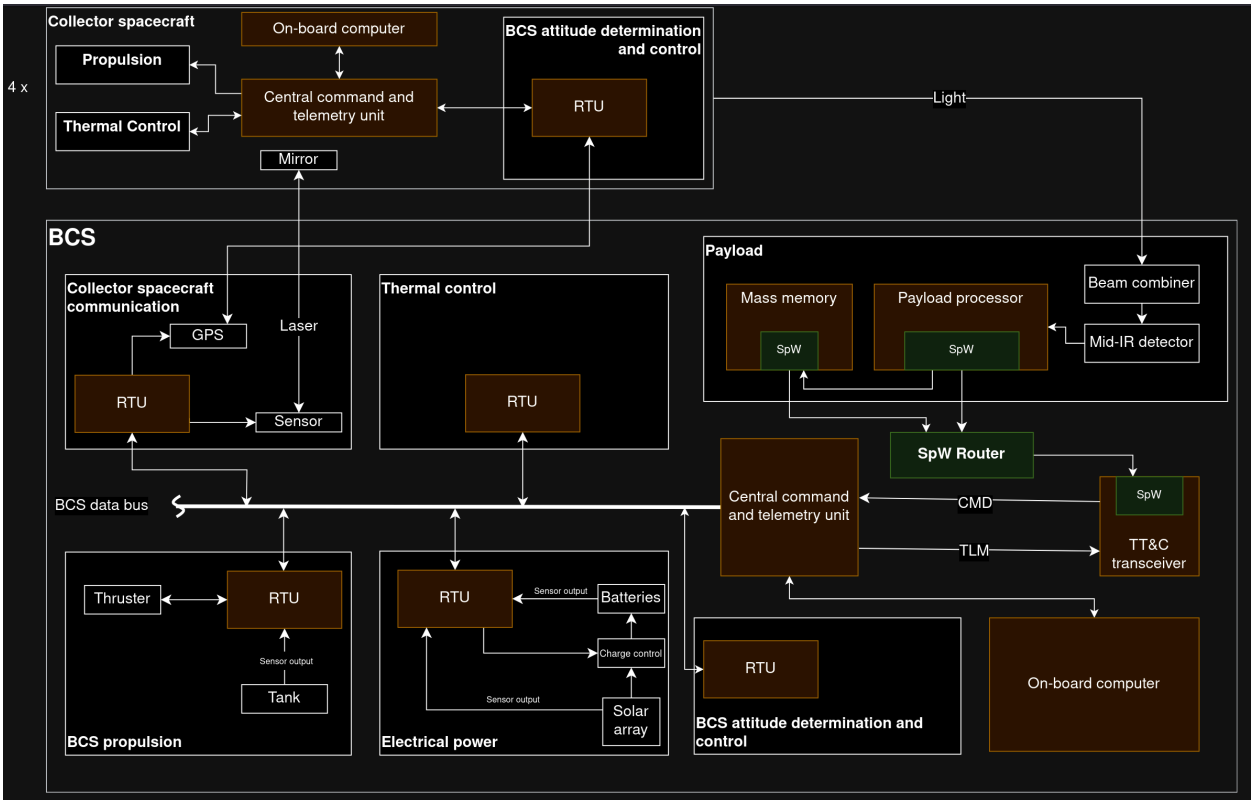

Figure 4: Block diagram of the on board data handling system

3.5 Propulsion

Contributed: Jim Vissers

The propulsion subsystem must perform the mid-course correction burns to ensure insertion in the desired halo orbit. Once there, the system must perform station-keeping maneuvers, formation flying maneuvers, momentum management and end-of-life disposal. The propulsion systems differ for the beam collector spacecraft and the collector spacecrafts. Each collector spacecraft will have a low thrust propulsion system that will perform the station-keeping and formation flying, while the beam collector spacecraft will have a (relatively) high thrust system to perform the mid-course correction burns. During these burns the collector spacecrafts will be physically linked to the beam collector. This way the five spacecrafts do not need to perform the course corrections individually, limiting possible complications.

3.5.1 High Thrust System

Contributed: Jim Vissers

As determined in section 3.1 the Δv needed for mid-course corrections is 70.5 m/s (12.6 m/s contingency included). To determine the required thrust we first did a rough mass estimation based on the JWST mirror mass. The JWST mirror weighs 28.3 kg/m^2, so with a mirror diameter of 2.5 m a single mirror would weigh 140 kg. JWST's total mass is about 3 times the mass of its mirror assembly [18]. With a 20% margin the mass of a single mirror satellite is about 500 kg, similar to an estimate for the DARWIN mission [19]. Although the

beam combiner spacecraft does not have a mirror, it has all the necessary science equipment so we assume it to also weigh roughly 500kg.

We assume that the acceleration JWST experienced during its mid-course burns is appropriate for this mission as well. JWST Δv changed by 24.3 m/s over the span of 80 minutes [4]. Assuming constant acceleration the spacecraft was subjected to 5 mm/s^2 of acceleration, for the spacecraft assembly to get the same acceleration (assuming a mass of 2500 kg) 12.7 N of thrust is required.

Several options are available in this thrust range. To perform a trade-off we looked at monopropellant and hypergolic bipropellant options as these are reliable, flight-proven systems [20]. Hydrazine and ammonium dinitramide (ADN) monopropellants, as well as hydrazine/NTO and MMH/NTO hypergolic propellants were investigated. To estimate the required propellant mass and volume we used the rocket equation:

$$\Delta \mathrm{v} = g_0 \cdot I_{sp} \ln \frac{M_0}{M_0 - M_p} \quad \Rightarrow \quad M_p = M_0 \left(1 - \exp\left\{\frac{-\Delta \mathrm{v}}{g_0 \cdot I_{sp}}\right\}\right) \tag{3}$$

With the respective values for specific impulse and density we arrive at the estimation show in table 10.

Table 10: Investigated propellants with mass and volume estimations.

Propellant	**I$_{sp}$[s]**	**Density [kg/m^3]**	**Mass [kg]**	**Volume [L]**
Hydrazine monopropellant [20]	230	1021	76.91	75.33
ADN monopropellant [21]	231	1225.2	76.58	62.50
MMH-NTO bipropellant [22]	336	1200	52.90	44.09
Hydrazine-NTO bipropellant [23]	339	1220	52.44	42.98

Purely in terms of propellant performance a hydrazine-NTO combination scores the best, but there is an issue that has to be accounted for. Hydrazine and MMH are highly carcinogenic. For this reason alternatives for hydrazine-based propellants are being developed by ESA and others[24]. ADN monopropellant is one of these proposed alternatives and outperforms hydrazine monopropellant in laboratory testing[21]. Using this 'greener' fuel avoids the high handling costs and potential health risks to personnel. For this reason it is selected as the propellant used by the high-thrust system. In this decision we assume there is ample time to develop this technology to a sufficient level. Thrusters are being developed in the 1-20 N range that use this new fuel[24] and installing four of them will provide enough thrust and some redundancy to the system.

3.5.2 Low Thrust System

Contributed: Martina Iacona

Our mission is composed of multiple spacecrafts forming a free-flying constellation and moving in a circular path, which allows for lower initial mass and lower power consumption for the propulsion system compared to a square flight path [25]. The operations that the spacecrafts need to perform in a free-flying constellation setup and that regard spacecraft orientation maintenance are:

1. Deployment in L2 orbit.
2. Pointing of the spacecraft towards the target star, with formation plane perpendicular to the target [19].
3. Adjusting the positions of the spacecrafts with respect to each other in order to achieve the wanted resolution, related to baseline length, of the virtual telescope.
4. Keeping the position of the spacecrafts set-up stable in order to perform nulling interferometry and observe the potential exoplanet spectrum.

5. Rotation of the spacecrafts' array to modulate the intensity of the planet signal. This allows to find the exoplanet despite the presence of exo-zodiacal dust emission, caused by the remnants of the protoplanetary disk around the star [26] (modulation frequency of the exo-zodiacal emission would be twice the modulation frequency of the planet signal making their discrimination possible [27]; more information of this in the Scientific Case Study Report in Subsection 3.5).

6. Reconfiguration of the spacecrafts when they have to point towards a new target star.

For the purposes stated in 3.5, we are looking for propulsion systems with low thrust. Based on Figure 5, the best options are cold gas, electro-thermal propulsion and electric propulsion systems. Among the electric propulsion systems, FEEP (Field Emission Electric Propulsion) and Hall effect thrusters are discussed candidates for both TPF and DARWIN missions [25], while ion thrusters are among the best candidates for the DARWIN mission [19]. For electro-thermal propulsion, resistojets are mentioned in the best candidates for the DARWIN mission [19].

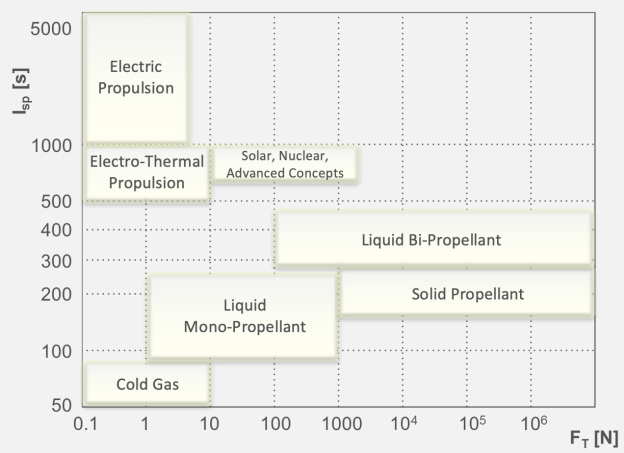

Figure 5: Specific impulse [s] vs. thrust [N] for the different propulsion systems [28]

In order to perform the previously listed operations, micro-newton propulsion and milli-newton propulsion techniques are needed. In particular, micro-newton thrusters are used for fine pointing, as pointing during fringe acquisition (step 2) and for optical path difference control during scientific observations (step 4) [19]. Milli-newton thrusters are used for formation deployment (step 1) & failure recovery, orbit maintenance manoeuvres, reconfiguration/resizing of the interferometer (step 5) and rotation of the interferometer (step 4) [19]. To understand which propulsion system performs the best among cold gas thrusters, FEEP, Hall effect thrusters, ion thrusters and resistojets, we made two trade-off tables: one for milli-newton propulsion systems (Figure 6) and one for micro-newton propulsion systems (Figure 7). In these tables, mass and volume have been calculated following the same procedure as the one used for high trust systems.

Milli-propulsion	Criteria	**Thrust**	**Volume**	**Mass**	**Power consumption**	**Payload contamination**	**Maturity of technology**	**Total**
	Weight	1	1	1	1	2	1	
Candidates	*Cold gas thrusters*	4	1	1	5	5	4	25
	FEEP	2	5	5	2	2	2	20
	Ion thrusters	2	4	5	3	4	5	27
	Hall-effect thrusters	2	4	4	1	4	2	21
	Resistojets	3	1	3	5	5	5	27

Figure 6: Trade-off table for milli-propulsion system

Micro-propulsion	Criteria	**Thrust**	**Volume**	**Mass**	**Power consumption**	**Payload contamination**	**Maturity of technology**	**Total**
	Weight	2	1	1	1	2	1	
Candidates	*Cold gas thrusters*	5	2	3	5	5	5	35
	FEEP	5	5	5	2	2	2	27
	Ion thrusters	4	5	5	3	4	5	34
	Hall-effect thrusters	1	5	5	1	4	1	23
	Resistojets	1	3	4	5	5	1	25

Figure 7: Trade-off table for micro-propulsion system

The marking system we used is based on the following table 11:

Table 11: Table used to mark the criteria for the propulsion trade-off tables

Milli-thrust	**Micro-thrust**	**Volume**	**Mass**	**Power consumption[19]**	**Payload contamination**	**Maturity of technology**	**Mark**
0.1-1 mN	0.1-10 µN	100-300L	80-100kg	>100W	Teflon	Recent development	1
0.1-55 mN	0.1-55 µN	50-100L	50-80kg	50-100W	Caesium	Fully developed: tested but not used	2
0.1-100 mN	0.1-100 µN	10-50L	10-50kg	30-50W	Other	Used in one mission	3
0.1-550 mN	0.1-550 µN	1-10L	5-10kg	15-30W	Ionised benign gas	Used in several missions	4
0.1-1000 mN	0.1-1000 µN	0.1-1L	0.1-5kg	0-15W	Benign gas, not ionised	Used in multiple missions with success	5

Based on the milli-propulsion analysis, the results are as follows:

1. FEEP (29 points);
2. Ion thrusters and resistojets (27 points);

3. Cold gas thrusters (25 points);
4. Hall effect thrusters (23 points).

Based on the micro-propulsion analysis, the results are:

1. Cold gas thrusters (35 points);
2. Ion thrusters (34 points);
3. FEEP (27 points);
4. Resistojets (25 points);
5. Hall-effect thrusters (23 points).

In order to save weight, we would like to use a single tank for both micro- and milli-propulsion systems. For this reason, our aim is to choose only one candidate across cold gas thrusters, FEEP, ion thrusters, Hall-effect thrusters and resistojets. Looking at the scores, ion thrusters, which are second in both rankings, or cold gas thrusters, which are first for micro-propulsion and third for milli-propulsion (even if they are third, the points difference with FEEP is only 4 points), seem to be the most reasonable choices. Cold gas thrusters main problem is the high mass (total of 99.5kg) and volume (total of 355.5kg); ion thrusters main problem is the relatively high power consumption (<50W[29]). Given that the launch vehicle can afford masses larger than 2500kg as discussed in 4, the amount of mass and volume required by cold gas thrusters are feasible. As a result, we arrived at the conclusion that cold gas thrusters are the best solution for our mission, in agreement with [19].

Number of thrusters
According to previous studies for the DARWIN mission [19], at least 8 thrusters should be placed on each mirror spacecraft to allow for attitude and position control of translation (3 degrees of freedom) and rotation (3 degrees of freedom). A proposed configuration consists of 16 thrusters placed in 2 different planes of the mirror spacecrafts (8 on a lower and 8 on a upper plane) [30].

Alternative technology
Propellant waste, contamination caused by plumes and carriage of large amount of propellants to ensure enough propellant for the entire mission lifetime can impose limitations to the mission. Therefore, a new concept has been developed specifically for the TPF mission.

The MIT Space Systems Lab (SSL) has been exploring electro-magnetic formation flight (EMFF) as an alternative method to adjust the relative orientations of the spacecrafts. EMFF is based on the principle of electromagnets coupled with reaction wheels [31]. Electromagnets consists of wires wound into coils, hence, by sending a current through the wire, a magnetic field will generate CITE. The magnetic field disappears when the current is turned off [32]. Experiments at the MIT Space Systems Lab tested the attraction, repulsion and sideways movement of the two spacecrafts, made possible by changing the current running through superconducting coils [33]. Ideally, by changing the orientation of the electromagnetic field, different forces produced in any direction can be used to move the spacecrafts in the desired configuration [34]. However, the downside of this method is that even if it does not use any propellant and there would, therefore, be no limit on the mission lifetime, the EMFF system uses solar power to energize a magnetic field [31]. Hence, a detailed analysis is needed to realize how much power is required to keep the spacecrafts in a stable configuration. Moreover, Earth's magnetic field and the spacecraft's internal magnetic field can introduce issues for keeping the stability. EMFF technique requires more studies and it is not yet ready to be used. Also, the articles available only take into account the case of two spacecrafts, which is not what our mission aims to. We do, however, think that this technique has great potential and that it can be used in the future.

3.6 Electrical Power Subsystem

Contributed: Jim Vissers

The electrical power subsystem (EPS) must generate and distribute power for the scientific payload and other subsystems. First the power required for the payload and different subsystems is estimated. Although there are significant differences between our mission and JWST in terms of operation (interferometry, formation-flying etc.) The power draw that the JWST sees is used as a reference[18]. The power draw for telecommunications is referenced in section 3.3. The power budget estimation is shown in table 12.

Table 12: Power draw estimation for beam combiner and telescope spacecraft

	Spacecraft	
Subsystem	Beam combiner	Telescope
Telescope assembly	N/A	30
Science module	240	N/A
Attitude control	180	180
Electrical power	60	60
CDHS	140	140
Telecommunication	147.4	32
Thermal control	400	50
Wiring harness	230	230
Propulsion	120	120
Total power draw [W]	1517.4	842

The solar flux present at the Earth-Sun L2 point is sufficient to utilize solar arrays for power generation. The L2 point is at 1.01AU from the sun thus by the inverse square law there is 1340 W/m^2 available. To size the array the lifetime degradation factor L_D of the panels has to be calculated. Degradation of the solar panels is driven by the radiation environment and can be estimated by:

$$L_D = (1 - \mathrm{DR})^t \tag{4}$$

Where DR is the yearly degradation rate and t the mission lifetime in years. With a conservative degradation rate of 1.5% per year for gallium arsenide (GaAs) solar cells operating in a geostationary orbit (which is assumed to be relatively similar radiation-wise as L2) and a mission lifetime of 5 years I get $L_d = 0.927$[35]. So after 5 years of operation 92.7% of the cells are still working. Since the orbit is such that no eclipses occur, a daytime path efficiency η_{path} of 80% is used. This accounts for losses in power distribution and management[35]. A solar cell efficiency η_{cell} of 40% for modern triple-junction cells is used[36]. The required solar array area can then be calculated by:

$$A_{\mathrm{array}} = \frac{P_{\mathrm{req}}}{L_d \cdot \eta_{\mathrm{path}} \cdot \eta_{\mathrm{cell}} \cdot S} \tag{5}$$

Where P_{req} is the required power and S the solar flux. For the beam combiner spacecraft the required area is 3.82m^2 and 2.05m^2 for the telescope spacecraft. In this estimation battery charging is not accounted for as they are only needed to provide power during the launch (the solar panels have to be in a stowed position). Each spacecraft will have a battery that can handle power draw during launch and eventual peak draws, but a more in-depth analysis is required for this.

3.7 Structures and Mechanisms

Contributed: Jim Vissers

The structures 'subsystem' must ensure structural integrity during all segments of the mission, as well as

facilitate attachment points for the payload and other subsystems. The mechanisms subsystem must ensure deployment and pointing for the payload, solar arrays and telecommunication.

The highest loads and critical vibrations are experienced during launch. As a reference for the loads and vibrations experienced by the spacecraft the launch manual of the Falcon 9 was consulted. During a launch the maximum axial acceleration is 6g, and lateral acceleration peaks at 2g. The natural frequency in axial direction should be kept above 25Hz and for the lateral direction above 10Hz [37]. The primary structure of the spacecraft must account for these loads. As a starting point a cylindrical tube (within and around which the secondary/tertiary structures are built) is considered. To estimate the radius of the cylinder, the radius of a spherical tank that can hold the nitrogen propellant was calculated. For a volume of 344L a radius of 43.5cm is required. To allow for some margin I take a radius of 0.7m. The tank would be 0.87m high and to allow for other systems the height of each spacecraft will be 1.25m. In the fairing these cylindrical sections will be stacked on top of each other, with the beam combiner at the bottom. This does pose a problem since the cylinder would have to through the telescope mirrors. For this estimation I will disregard this, but an alternative storing configuration or primary structure would have to be designed.

The primary structure will be a thin-walled cylinder with a 0.7m radius and 5.25m height. I investigated four materials commonly used in spacecraft structures: two alloys of aluminium, a high-grade steel alloy and titanium [38].The mass of the the spacecraft is treated as a point mass at the end of a beam and weighs 2500kg. I used the following equations to estimate the thickness of material needed to ensure axial and lateral stiffness, strength and resistance to buckling[35]:

$$\text{axial: } f_n = \frac{1}{2\pi}\sqrt{\frac{EA}{ML}} \quad \text{lateral: } f_n = \frac{1}{2\pi}\sqrt{\frac{3EI}{ML^3}} \tag{6}$$

$$\text{strength: } \sigma = g_{ax}\frac{M}{A} + g_{lat}\frac{MLR}{I} \quad \text{buckling: } \frac{\sigma_{cr}}{E} = 9\left(\frac{t}{R}\right)^{1.6} + 0.16(t/L)^{1.3} \tag{7}$$

With a thin wall approximation the cross-sectional area A becomes $2\pi Rt$ and moment of inertia I is $\pi R^3 t$. Using these techniques the wall thickness and mass was estimated as shown in table 13.

Table 13: Mass estimate for different materials

Material	**E [GPa]**	ρ **[kg/mˆ3]**	σ_y **[MPa]**	**Thickness [mm]**	**Mass [kg]**
Aluminium AA6061	68.9	2700	310	1.069	66.626
Aluminium AA2024	72.0	2780	345	1.023	65.646
Steel D6AC	210	7870	1724	0.351	63.717
Titanium	114	4430	880	0.646	66.069

The thickness needed to remain above the axial stiffness constraint was leading and is shown in the table. When performing the buckling check it showed that with these thicknesses all materials except steel fail. With steel being the most lightweight option (even without the other materials being strengthened for buckling) it is a clear winner in this case. Other space missions that use this metal as a primary structural member were not found and its corrosion resistance in a space environment must be further investigated.

The secondary structure must house the other subsystems and offer some protection from micrometeorites and radiation [35]. The attachment points for the antennas and solar panel will also be on the secondary structure. This outer shell will be a cube 1.2 on the sides and 0.6m in height. The shell is commonly made of aluminium but this metal would form a galvanic coupling with the primary structure's steel, meaning an alternative will have to be investigated [39].

3.8 Thermal Control

Contributed: Bradut Stanciu

The thermal control subsystem of the proposed final design of the spacecrafts is based upon the James Webb design due to the similarities in mission profile as well as the instrumentation used for the observation of the exoplanets. As such, at a conceptual level, it is known that a sunshield will be necessary in order to keep the mirrors at a temperature of 40 Kelvin to be able to reflect the coming infrared emissions and a cryocooler shall be required to be able to keep the temperature of the detector below the required temperature of 7K [40]. The sunshield shall be designed by assuming that the spacecraft bus, the sunshield itself and the telescope are thermally decoupled, in order to enable a simplified analysis of the sunshield itself. Another assumption is that the heat emitted by the spacecraft bus itself shall be considered insignificant compared to the heat emitted by solar radiation. Additionally, as in the case of the James Webb the sun facing side of the sunshield for the first two layers shall use silicon Kapton film whereas the telescope facing side shall use Double aluminized Kapton. The optical properties of these 2 materials shall be presented below:

Table 14: Absorbtivity and emissivity of two Kapton materials

Material	**Absorbtivity**	**Emissivity**	**Source**
Silicon Kapton	0.13	0.75	[41]
Aluminized Kapton	0.09	0.03	[42]

Thus, assuming a Solar Irradiance of 1317 Watts at the Lagrangian point and considering the fact that the heat emitted by the spacecraft bus is not taken into account the equilibrium temperature of the first layer of the sunshield can be calculated by using the following formula:

$$T_1 = \left(\frac{\alpha \cdot S}{(\epsilon_{Sil} + \epsilon_{Kap}) \cdot \sigma} \right)^{0.25} \tag{8}$$

where α represents the absorbtivity of the sunlit side of the first layer (0.13), S represents the value of the solar flux(1317 Watt) and σ represents the Boltzmann constant ($5.67 \cdot 10^{-8}$).
Thus, the first layer has an equilibrium temperature of 249.4 Kelvin. Using this equilibrium temperature, the emitted heat by the first layer towards the detector can be determined to be equal to:

$$Q_1 = T_1^4 \cdot \sigma \cdot \epsilon_{Kap} \cdot A \tag{9}$$

Thus, the emitted heat is equal to a value of 6.585 Wm^{-2}. This emitted heat can then be used to determine the equilibrium temperature of the 2nd layer using the following formula:

$$T_2 = \left(\frac{Q_1}{(\epsilon_{Sil} + \epsilon_{Kap}) \cdot \sigma} \right)^{0.25} \tag{10}$$

This yields an equilibrium temperature of 110.46 Kelvin. Then, the emitted heat of the 2nd layer can then be calculated as such:

$$Q_2 = T_2^4 \cdot \sigma \cdot \epsilon_{Kap} \cdot A \tag{11}$$

Thus, the emitted heat of the 2nd layer is equal to a value of 0.253 Wm^{-2}. From the 3rd layer onwards the equilibrium temperature can be determined using the following formula:

$$T_n = \left(\frac{Q_{n-1}}{\epsilon_{Kap} \cdot \sigma} \cdot 2 \right)^{0.25} \tag{12}$$

Lastly, the emitted heat can be determined to be the following:

$$Q_3 = T_3^4 \cdot \sigma \cdot \epsilon_{Kap} \cdot A \tag{13}$$

Thus it can be deduced that each layer added after the 3rd layer halves the emitted heat received by the next layer since both sides of the sunshield layer are made of the same material.

Thus, based on the desired final layer equilibrium temperature, the minimum number of layers required can be determined. Based on the fact that the mirrors require a temperature below 40 Kelvin as in James Webb, this temperature shall be assumed to be the desired layer temperature. Finally, the number of layers added after the 3rd layer can be calculated with the following formula considering the fact that the emitted heat halves with each added layer from the 3rd layer:

$$n_{layers} = \ln(Q_3/Q_T)/\ln(2) \tag{14}$$

where Q_T is equal to the heat emitted by a layer at equilibrium temperature (40 K).

Thus, using this formula it is clear that the sunshield has to have a total of 5 layers in order to reach an equilibrium temperature lower than 40 Kelvin. Due to fluctuations in temperature in actual conditions, a further 2 layers shall be added for redundancy, leading to a sunshield consisting of 7 layers.

However, assuming that the instrument has an internal heat load of 1 Watt and a total emissivity of 1.1(assuming high emissivity on the detector side , as close to 1 as possible, and low emissivity on the sunshield side around 0.1), then the instrument temperature can be calculated to be approximately equal to 63K despite an equilibrium temperature of the 7th layer of 24.45 Kelvin. This leads to the conclusion that a cryocooler is necessary in order to enable the detector to reach the required 7K temperatures. Assuming that a similar design to the James Webb MIRI cryocooler is employed, a heat load of 400 Watts can be expected to be required for dissipation by the spacecraft bus [43].

Additionally, the heat load of the spacecraft bus subsystems except the cryocooler can be approximated to be in the best case scenario approximately equal to 40% of the total required electrical power [44]. As such, the total power required to be emitted can be determined to be equal to $Q_{int} = 400 + 0.4 * P_e$ and as such for the telescope spacecraft the internal heat is equal to 764 Watts. However, in the case of the mirror-carrying spacecraft, there is no need for cryocooling and as such $Q_{int} = 0.4 \cdot P_e$. Thus, the internal heat has a value of 280 Watts.

Lastly, in order to simplify the design and optimize weight, deployable radiators shall be used to radiate the excess heat [45]. As such, the entire spacecraft bus structure shall be covered in Alluminized Kapton multilayer insulation which has the optical properties as presented in the sunshield layers. Moreover, the radiators can be assumed to have an absorbtivity of 0.2 and an emissivity of 0.8 based on typical optical properties of radiators [46].

Using the aforementioned solar flux of 1317 Watts, the solar heat can also be calculated as:

$$Q_{sun} = S \cdot x \cdot y \tag{15}$$

where x and y represent the bus dimensions and are equal to 1.2 meters each. This assumes that the sunlight is perpendicular to the -z surface. Thus, the sunlight heat has a value of 75.85 Watts.

Additionally, it can be considered that all the subsystems of the spacecraft operate at around 300 Kelvin considering that this is the operational temperature for the subsystems on the James Webb [47], that typically all electronic components also function at 300 Kelvin [48] and that the chosen propellants can also be safely stored in that temperature range [49][50].

Taking into account static thermal equilibrium, we can as such assume the spacecraft equilibrium temperature to be equal to 300 Kelvin, in order to be able to size the radiators properly. Thus, the area of the radiators

can be determined using the following equation:

$$A_{rad} = \frac{Q_{sun} + Q_{int} - Q_{bus}}{T_0^4 \cdot \epsilon_{rad} \cdot \sigma} \tag{16}$$

where $Q_{bus} = A_{bus} \cdot \epsilon_{MLI} \cdot \sigma \cdot T_0^4$ with $T_0 = 300K$ and A_{bus} represents the surface area of the spacecraft bus. With the use of Equation 16, the area of the radiators can then be determined to be equal to 2.327 m^2 for the telescope spacecraft and 1.0106 m^2 for the mirror spacecraft.

As such, the proposed thermal control system of our spacecraft consists of a 7-layer sunshield and a cryocooler used to decrease the detector temperatures to the required 7 Kelvin temperature, as well as Aluminized Kapton MLI and deployable radiators to keep the detector spacecraft in operating range temperatures. In the case of the mirror-carrying spacecraft, the thermal control is composed only of a 7-layer sunshield and Aluminized Kapton MLI and deployable radiators.

4 Launch vehicle

Contributed: Pieter van Zoelen

There are a number of requirements we have to meet for the launch vehicle: it needs to be able to launch enough mass to the L2 transfer orbit which has a characteristic energy of $C3 = -0.7$ km^2 s^{-2}, it needs to be able to fit our satellites and it needs to fit in our budget [51]. In table 15 current and announced launchers capable of delivering payloads to L2 are listed (with exception of Russian and Chinese launchers):

Table 15: List of launch vehicle options. Note: SLS mass is to Earth escape trajectory (C3 = 0 km^2 s^{-2}) and F9 (expendable) mass is to trans-Mars injection (C3 = 8–12 km^2 s^{-2}), the actual possible payload mass is higher. The NASA Launch Vehicle Performance Calculator gave inconsistent values for New Glenn but we have been unable to find other values, the actual possible payload mass is likely higher. Fairing dimensions are external dimensions, payload space is smaller. Costs for SLS, Vulcan Centaur and Starship are estimates. Starship payload mass is an estimate based on its LEO and GTO capabilities, the upper cost limit is based on the Falcon Heavy cost. It is unclear if the Falcon recovery options are cheaper than expendable options.

Launch vehicle	**Mass to L2**	**Cost (millions)**	**Fairing (⌀, height)**	**Source**
Ariane 62	3300 kg	€75	5.4 m, 14 or 20 m	[52][53]
Ariane 64	8000 kg	€115	5.4 m, 20 m	[52][53]
Falcon 9 (Recovery)	3390 kg	$67	5.2 m, 13.2 or 18.7 m	[54][37][55]
Falcon 9 (B5, Expendable)	4020 kg	$67	5.2 m, 13.2 or 18.7 m	[37][55]
Falcon Heavy (Expendable)	15220 kg	$97	5.2 m, 13.2 or 18.7 m	[54][37][55]
Falcon Heavy (Recovery)	6820 kg	$97	5.2 m, 13.2 or 18.7 m	[54][37][55]
New Glenn	7145 kg	Unknown	7 m, 21.9 m	[54][56]
Space Launch System (B1)	26600 kg	$500 – ≥2000	5.1 m, 19.1 m	[57][58][59]
Space Launch System (B1B)	37000 kg	Unknown	8.4 m, 19.1 m	[57]
Space Launch System (B2)	44300 kg	Unknown	8.4 m, 27.4 m	[57]
Starship (Expendable)	70000 kg	$10 – 100	8 m, 22 m	[60][61][62]
Vulcan Centaur (VC0)	2160 kg	$100 – 200	5.4 m, 15.5 or 21.3 m	[54][63][64]
Vulcan Centaur (VC2)	6010 kg	$100 – 200	5.4 m, 15.5 or 21.3 m	[54][63][64]
Vulcan Centaur (VC4)	8655 kg	$100 – 200	5.4 m, 15.5 or 21.3 m	[54][63][64]
Vulcan Centaur (VC6)	10975 kg	$100 – 200	5.4 m, 15.5 or 21.3 m	[54][63][64]

Our spacecraft design is similar to that of the Darwin and Terrestial Planet Finder (TPF) constellations. Using the mass based on Darwin and JWST of 2500 kg (see subsubsection 3.5.1) and including a 20% margin bringing the mass to 3000 kg, we see that only the VC0 variant of the Vulcan Centaur is not an option. This leaves us with a wide variety of possible launch vehicles. We can also safely say that SLS is too expensive, potentially being more than twice as expensive than our combined budget for spacecraft and mission. We will not consider New Glenn because no cost information is available.

In terms of volume, we know the five satellites of the TPF could fit in the Ariane 5 ECA [65]. Assuming our volume will be similar, we do not run into any problems with any of the remaining launch options. Assuming 2.5m diameter primary mirrors, our mirrors can be monolithic since they can fit unfolded in all launchers.

At this point we have the luxury of being able to choose. Because of our strained budget Starship appears to be our best option in terms of cost if we are optimistic, but the more flight-proven Falcon 9 launch vehicle is close to that cost and known to be very reliable. If we reserve $67 million or €62 million for the launcher we can choose between the Falcon 9 (recoverable), Falcon 9 (expendable), and Starship if the cost of the latter becomes lower than that of the Falcon 9.

5 Cost estimate

Contributed: Pieter van Zoelen

Because we have not looked at every component in-depth, it is hard to say what the exact cost of the spacecraft is likely to be. However, we know that our mission is similar to the Darwin mission both in terms of mass and technology, and that Darwin has a cost estimate in the mission proposal [15]. There, the following cost estimates are used which we have corrected for inflation in table 16:

Table 16: Darwin cost estimate (2007) corrected for inflation. Spacecraft cost per kg includes 15% margin.

Category	**Darwin estimate**	**Inflation corrected**
Spacecraft	845 M€	1187 M€
Launcher	125 M€	176 M€
Ground services (5 years)	55 M€	77 M€
Pre-implementation cost	1% of total costs	
Space agency internal costs	11% of total costs	
Total cost	1165 M€	1636 M€

The launcher considered for the Darwin mission was an Ariane 5 ECA [15]. Using our €62 million launch vehicle estimation (see section 4), we get to a total cost estimate of €1507 million. In the following table this cost is compared to our budget:

Table 17: Allocated mission budget compared to expected costs based on the Darwin mission.

Category	**Budget**	**Expectation**	**Difference**
Spacecraft	100 M€	1187 M€	1087 M€
Mission	900 M€	320 M€	-580 M€
Total	1000 M€	1507 M€	507 M€

We can see that the spacecraft is massively over budget at 1187% of the budget, while the rest of the mission is only at 36% of the budget. In total this brings our expected cost to €507 million over (or 151% of) the total budget. Because there are no obvious ways of reducing this cost without compromising the requirements such as the number of planets our mission is required to detect, we advise our mission client to reassign part of the mission budget to the spacecraft and to allocate extra funding.

References

[1] Oswald Wallner et al. "DARWIN mission and configuration trade-off". In: *Proceedings of SPIE - The International Society for Optical Engineering* 6268 (June 2006). DOI: 10.1117/12.671658.

[2] Charles Cockell et al. "Darwin —A Mission to Detect and Search for Life on Extrasolar Planets". In: *Astrobiology* 9 (Mar. 2009), pp. 1–22. DOI: 10.1089/ast.2007.0227.

[3] Lisa Kaltenegger et al. "Target star catalogue for DARWIN: nearby habitable star systems". In: *IAU Colloq. 200: Direct Imaging of Exoplanets: Science & Techniques*. 2006, pp. 89–92.

[4] Karen Richon, Jeremy Petersen, and Ann Nicholson. "Flight Dynamics Planning and Operations Support for the JWST Mission". In: 2022 AAS/AIAA Astrodynamics Specialist Conference. Report number AAS 22-611. July 2022. URL: https://ntrs.nasa.gov/citations/20220010259.

[5] Space Telescope Science Institute. *JWST Orbit - JWST User Documentation*. July 2022. URL: https://jwst-docs.stsci.edu/jwst-observatory-characteristics/jwst-orbit.

[6] Jeffrey Y. Tien et al. "Relative Sensor with 4Pi Coverage for Formation Flying Missions". In: 2nd International Symposium on Formation Flying Missions and Technologies. Sept. 2004. URL: https://ntrs.nasa.gov/citations/20060048517.

[7] NASA Goddard Space Flight Center and S.R. Starin. "Attitude Determination and Control Systems". In: *NASA Goddard Space Flight Center* (2011). URL: https://ntrs.nasa.gov/api/citations/20110007876/downloads/20110007876.pdf.

[8] Bin Yang et al. "DOA estimation for attitude determination on communication satellites". In: *Chinese Journal of Aeronautics* 27.3 (2014), pp. 670–677. ISSN: 1000-9361. DOI: https://doi.org/10.1016/j.cja.2014.04.010. URL: https://www.sciencedirect.com/science/article/pii/S1000936114000806.

[9] *JWST Fine Guidance Sensor - JWST User Documentation*. Mar. 2020. URL: https://jwst-docs.stsci.edu/jwst-observatory-hardware/jwst-fine-guidance-sensor.

[10] *JWST Telescope - JWST User Documentation*. Dec. 2022. URL: https://jwst-docs.stsci.edu/jwst-observatory-hardware/jwst-telescope.

[11] Space Telescope Science Institute. *JWST Communications Subsystem*. 2023. URL: https://jwst-docs.stsci.edu/jwst-observatory-hardware/jwst-spacecraft-bus/jwst-communications-subsystem (visited on 01/07/2024).

[12] Wikipedia. *Radio Window*. Accessed: 2024-01-07. 2024. URL: https://en.wikipedia.org/wiki/Radio_window.

[13] Gerard Janssen. *Telecommunications*. Lecture notes in Electrical Engineering. Lecture series. 2023.

[14] Dr. Alessandra Menicucci. *On-board command and data handling [lecture slides]*. 2023.

[15] Alain Leger and Tom Herbst et al. *Darwin Science Across Disciplines: A proposal for the Cosmic Vision 2015-2025 ESA Plan*. July 2007. arXiv: 0707.3385 [astro-ph].

[16] Alan Johns et al. "James Webb Space Telescope: L2 communications for science data processing". In: *Observatory Operations: Strategies, Processes, and Systems II*. Vol. 7016. SPIE. 2008, pp. 425–431.

[17] July 2020. URL: https://www.star-dundee.com/spacewire/getting-started/an-overview-of-the-spacewire-standard/.

[18] M. Menzel and M. Davis. *The Design, Verification, and Performance of the James Webb Space Telescope*. Tech. rep. NASA, 2023.

[19] M. Kilter. "Micropropulsion Technology Assessment for DARWIN". MA thesis. Luleå University of Technology, 2004.

[20] *Orbital Propulsion Centre*. URL: https://www.space-propulsion.com/index.html.

[21] K. Anflo, P. Thormählen, and M. Persson. *Hot-Firing tests using a low temperature derivative of LMP-103S*. Tech. rep. ECAPS, 2013.

[22] *N2O4/MMH*. URL: http://www.astronautix.com/n/n2o4mmh.html.

[23] *N2O4/Hydrazine*. URL: http://www.astronautix.com/n/n2o4hydrazine.html.

[24] ESA. *Considering hydrazine-free satellite propulsion*. 2013. URL: https://www.esa.int/Space_Safety/Clean_Space/Considering_hydrazine-free_satellite_propulsion.

[25] A. Kurt et al. "Plasma Propulsion Options for Multiple Terrestrial Planet Finder Architectures". In: *JOURNAL OF SPACECRAFT AND ROCKETS* (2002). URL: https://web.archive.org/web/20100624160200id_/http://alfven.princeton.edu/papers/JSCandR.pdf.

[26] Daniel Rouan. "Nulling Interferometry". In: *Springer, Berlin, Heidelberg* (2022). Encyclopedia of Astrobiology, pp.1–5. URL: https://link.springer.com/referenceworkentry/10.1007/978-3-642-27833-4_1088-3.

[27] Julien Felix Paul Spronck. "The Role of Amplitude, Phase, Polarization and their Interconnection in Nulling Interferometry". Doctoral thesis. TU Delft, 2008. URL: https://repository.tudelft.nl/islandora/object/uuid:12fe697e-9ae2-44c7-bdc8-95bce2e783e8.

[28] Angelo Cervone. "Space propulsion". From lecture of AE3524: Spacecraft Design and Astrodynamics.

[29] I S Vavilov et al. "Review of electric thrusters with low consumption power for corrective propulsion system of small space vehicles". In: *Journal of Physics: Conference Series* (2020). DOI: 10.1088/1742-6596/1546/1/012071. URL: https://iopscience.iop.org/article/10.1088/1742-6596/1546/1/012071/pdf.

[30] V. Pizzagalli et al. "DARWIN MISSION THE FIELD EMISSION ELECTRIC PROPULSION (FEEP) OPTION". In: *Proceedings of the 4th International Spacecraft Propulsion Conference (ESA SP-555). 2-9 June, 2004, Chia Laguna (Cagliari), Sardinia, Italy. Editor: A.Wilson. Published on CDROM., id.84.1* (2004). URL: https://articles.adsabs.harvard.edu/pdf/2004sppr.confE..84P.

[31] Wikipedia. *Electromagnetic formation flight*. 2007. URL: https://en.wikipedia.org/wiki/Electromagnetic_formation_flight.

[32] Wikipedia. *Electromagnet*. 2002. URL: https://en.wikipedia.org/wiki/Electromagnet.

[33] Magnets help spacecraft fly in formation. *David Shiga*. 2008. URL: https://www.newscientist.com/article/dn13846-magnets-help-spacecraft-fly-in-formation/.

[34] David W. Miller et al. *Electromagnetic Formation Flight*. Tech. rep. Massachusetts Institute of Technology, Department of Aeronautics and Astronautics. URL: https://www.niac.usra.edu/files/studies/final_report/793Miller.pdf.

[35] B.T.C. Zandbergen. *Aerospace Design & Systems Engineering Elements I Part: Spacecraft (bus) design and sizing*. 2020.

[36] J. Li, A. Aierken, and Y. Liu. "A Brief Review of High Efficiency III-V Solar Cells for Space Application". In: *Frontiers* (2021). URL: https://www.frontiersin.org/articles/10.3389/fphy.2020.631925/full.

[37] Space Exploration Technologies Corp. *Falcon User's Guide*. Sept. 2021. URL: https://www.spacex.com/media/starship_users_guide_v1.pdf.

[38] Aerospace Specification Metals. *Aluminum 6061-T6; 6061-T651*. URL: https://asm.matweb.com/search/SpecificMaterial.asp?bassnum=ma6061t6.

[39] M.D. Danford and R.H. Higgins. *Galvanic Coupling Between D6AC Steel, 6061-T6 Aluminium*. Tech. rep. NASA, 1983.

[40] D Durand et al. "Mid InfraRed Instrument (MIRI) cooler subsystem design". In: *Cryocoolers* 15 (2009), pp. 7–12.

[41] Wei Xiao et al. "Flexible thin film optical solar reflectors with Ta2O5-based multimaterial coatings for space radiative cooling". In: *APL Photonics* 8.9 (2023).

[42] John H Henninger. *Solar absorptance and thermal emittance of some common spacecraft thermal-control coatings*. Vol. 1121. National Aeronautics, Space Adminitration, Scientific, and Technical ..., 1984.

[43] Konstantin Penanen et al. *Mid-Infrared Instrument Cryocooler on James Webb Space Telescope: Cooldown, Commissioning and Initial Performance.* 2022.

[44] Boris Yendler, Ashton Meginnis, and Adam Reif. "Thermal management for high power Cubesats". In: (2020).

[45] Fabian Preller et al. "Deployable Passive Radiator Development". In: 51st International Conference on Environmental Systems. 2022.

[46] W.J.Larson and J.R.Wertz. *Space Mission Analysis and Design*. 3rd ed. P.O. Box 17, 3300 AA Dordrecht, The Netherlands.: Microcosm Press and Kluwer Academic Publishers, 2005.

[47] GS Wright et al. "The mid-infrared instrument for the james webb space telescope, ii: Design and build". In: *Publications of the Astronomical Society of the Pacific* 127.953 (2015), p. 595.

[48] Hume Peabody. "Thermal Design for Spaceflight Fall 2022". In: (2023).

[49] K Anflo, T Gronland, and N Wingborg. "Development and testing of ADN-based monopropellants in small rocket engines". In: *36th AIAA/ASME/SAE/ASEE Joint Propulsion Conference and Exhibit*. 2000, p. 3162.

[50] Joseph Cardin and Jesus Acosta. "Design and test of an economical cold gas propulsion system". In: (2000).

[51] Mark Beckman and Leigh Janes. "Finding Acceptable James Webb Space Telescope Misson Orbits From a Fixed Ariane Flight Profile". In: AIAA/AAS Conference. Report number AAS-05-271. Jan. 2005. URL: https://ntrs.nasa.gov/citations/20050210121.

[52] ArianeSpace SA. *Ariane 6 User's Manual*. Feb. 2021. URL: https://www.arianespace.com/wp-content/uploads/2021/03/Mua-6_Issue-2_Revision-0_March-2021.pdf.

[53] Dominique Gallois. *Ariane 6, un chantier européen pour rester dans la course spatiale*. Dec. 2014. URL: https://www.lemonde.fr/economie/article/2014/12/01/les-europeens-s-appretent-a-mettre-ariane-6-en-chantier_4532259_3234.html (visited on 01/04/2024).

[54] *NASA Launch Services Program (LSP) Performance Web Site*. Nov. 2023. URL: https://elvperf.ksc.nasa.gov.

[55] Space Exploration Technologies Corp. *Capabilities & Services*. Mar. 2022. URL: https://web.archive.org/web/20230227145305/https://www.spacex.com/media/Capabilities&Services.pdf.

[56] L.P. Blue Origin Enterprises. *New Glenn Payload User's Guide*. Aug. 2018. URL: https://yellowdragonblogdotcom.files.wordpress.com/2019/01/new_glenn_payload_users_guide_rev_c.pdf.

[57] David Alan Smith. *Space Launch System (SLS) Mission Planner's Guide*. June 2017. URL: https://ntrs.nasa.gov/citations/20170005323.

[58] Origins Space Telescope Study Team. *Origins Space Telescope Mission Concept Study Report*. Aug. 2019. URL: https://asd.gsfc.nasa.gov/firs/docs/OriginsVolume1MissionConceptStudyReport_11Oct2019.pdf.

[59] Office of Management and Budget. *Letter to the Chair and Vice Chair of the Senate Appropriations Committee with respect to 10 of the FY 2020 annual appropriations bills*. Oct. 2019. URL: https://www.whitehouse.gov/wp-content/uploads/2019/10/shelby-mega-approps-10-23-19.pdf.

[60] Space Exploration Technologies Corp. *Starship Payload Guide*. Mar. 2020. URL: https://www.spacex.com/media/starship_users_guide_v1.pdf.

[61] Space Exploration Technologies Corp. *Starship*. URL: https://www.spacex.com/vehicles/starship/ (visited on 01/04/2024).

[62] Kate Duffy. *Elon Musk says he's 'highly confident' that SpaceX's Starship rocket launches will cost less than $10 million within 2-3 years*. Business Insider, Feb. 2022. URL: https://www.businessinsider.com/elon-musk-spacex-starship-rocket-update-flight-cost-million-2022-2.

[63] LLC United Launch Alliance. *Vulcan Launch Systems User's Guide*. Oct. 2023. URL: https://www.ulalaunch.com/docs/default-source/rockets/2023_vulcan_user_guide.pdf.

[64] Andrea Shalal and Irene Klotz. *'Vulcan' rocket launch in 2019 may end U.S. dependence on Russia*. Apr. 2015. URL: https://www.reuters.com/article/lockheed-boeing-rockets/vulcan-rocket-launch-in-2019-may-end-u-s-dependence-on-russia-idUSL2N0XA2DE20150414/.

[65] Stefan R. Martin et al. *TPF-I Emma X-array : 2007 design team study*. Pasadena, CA : Jet Propulsion Laboratory, National Aeronautics and Space Administration, 2007. DOI: 2014/40342. URL: https://hdl.handle.net/2014/40342.